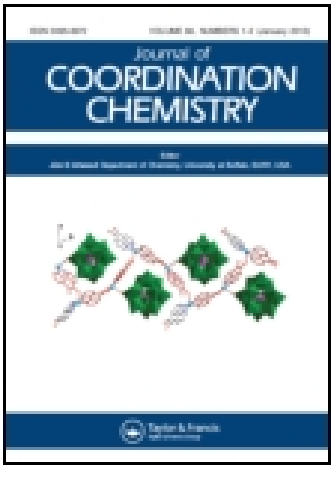

Journal of Coordination Chemistry
Publication details, including instructions for authors and subscription information:
http://www.tandfonline.com/loi/gcoo20

Solid state and theoretical study of structural properties induced by step-wise chloro functionalization in dicarbonyl-[2-(phenylamino)pent-3-en-4-onato]rhodium(I) complexes

Gertruida J.S. Venter[a], Gideon Steyl[a] & Andreas Roodt[a]
[a] Department of Chemistry, University of the Free State, Bloemfontein, South Africa

Accepted author version posted online: 10 Jan 2014.Published online: 05 Feb 2014.

Journal of Coordination Chemistry, 2014
Vol. 67, No. 1, 176–193, http://dx.doi.org/10.1080/00958972.2013.878801

Solid state and theoretical study of structural properties induced by step-wise chloro functionalization in dicarbonyl-[2-(phenylamino)pent-3-en-4-onato]rhodium(I) complexes

GERTRUIDA J.S. VENTER, GIDEON STEYL and ANDREAS ROODT*

Department of Chemistry, University of the Free State, Bloemfontein, South Africa

(*Received 5 September 2013; accepted 20 November 2013*)

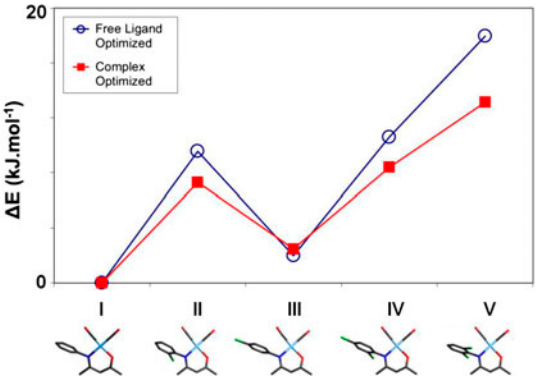

A series of five rhodium(I) dicarbonyl complexes containing systematically introduced phenyl-chloro substituted mono-anionic *β*-enaminoketonato ligands (N,O-bidentate donors) are presented. The influence of chloro substitution on the phenyl ring was investigated in the solid state and by theoretically optimized structures. Chloro substitution on the phenylamino ring in dicarbonyl [2-(phenylamino)pent-3-en-4-onato]rhodium(I) complexes were thus investigated with regard to optimized energies, metal–metal interactions, and bonding distances and angles primarily using X-ray diffraction and DFT calculations. The five complexes crystallized in three different crystal systems and five separate space groups. The packing modes of the complexes were evaluated by considering the relative orientation and metal–metal interactions and were found to be influenced by different factors, including weak intermolecular hydrogen bonds. Although no significant Cl···Cl interactions were observed, significant Rh···Rh bonding was identified. The theoretically optimized structures correlate very well with the solid state, with RMS overlay values varying between 0.62 and 0.23 Å. Upon coordination, the phenyl ring of the enaminato ligand adopts, without exception, an approximately 90° dihedral angle relative to the coordination plane, inducing a significant corresponding steric hindrance at the metal center. This is manifested by the complete blocking out of the well-known iodomethane oxidative addition reaction.

Keywords: Dicarbonyl; Rhodium(I); Enaminoketonato; Chloro interactions; Rh–Rh Interactions; DFT; Steric bulk

*Corresponding author. Email: roodta@ufs.ac.za

1. Introduction

Halogens may act as monodentate or bridging ligands in transition metal complexes or substituents in organic compounds. The steric accessibility of halogens has potential applications in supramolecular chemistry and crystal engineering [1, 2], wherein they are directly involved in forming intermolecular interactions. The effect of halogen bonding, and specifically chloro···chloro interactions, was first described by Schmidt [3–5] and is of interest in packing arrangements of halogenated compounds. It may be important when chloro substituents in aromatic compounds are present and contribute to stacking arrangements with a resultant short (*ca*. 4 Å) crystallographic axis [6]. A chloro···chloro contact may be characterized by the geometric parameters (θ_1, θ_1 and r_i) of the C_1–Cl_1···Cl_2–C_2 moieties (where $\theta_1 = C_1$–Cl_1···Cl_2, $\theta_2 = Cl_1$···Cl_2–C_2 and $r_i = X_1$···X_2 distance) [7, 8]. Cl···Cl close contacts are organized into two classes, Type I where $\theta_1 \sim \theta_2$ and Type II where $\theta_1 \sim 90°$ and $\theta_2 \sim 180°$ [8]. The distance r_i is classified as "close" when it is shorter than the sum of the van der Waals radii of the two chloro substituents, i.e. 3.5 Å (using the CSD standard van der Waals radius for Cl as 1.75 Å [9]). These M–Cl···X–C interactions have been systematically studied by Zordan *et al*. [10], demonstrating the role of the inorganic chloro (M–Cl) and the organic halogen (C–X) in selected transition metal compounds. The ability to introduce electron donating or withdrawing substituents increases the range of applications in transition metal chemistry.

Rhodium(I) dicarbonyl complexes of the type [Rh(L,L′-Bid)$(CO)_2$] with chelating monoanionic L,L′-bidentate ligands coordinated to rhodium via (O,O′) donors have been studied as catalyst precursors [11–13], with a well-known ligand of this type in [Rh(O,O′-Bid)$(CO)_2$] complexes being acetylacetone [14]. The application of similar ligands, also when combined with P-donor groups in basic catalytic reactions and related systems, have been described previously by our group [15–28].

Some dicarbonyl complexes of rhodium(I) with ring-forming ligands in their structure display short metal–metal bonds between parallel planar [Rh(L,L′-Bid)$(CO)_2$] fragments, imparting interesting optical (dichroism, metallic luster) and electrical (anisotropic conductivity) properties [29]. Rhodium···rhodium interactions have been correlated previously in [Rh(L,L′-Bid)$(CO)_2$] for the acetylacetonato and trifluoroacetylacetonato complexes [14] as well as compounds with ligands containing donors other than oxygen [30].

In the current study, investigation of these *β*-diketonato complexes is expanded to include complexes containing bidentate *β*-enaminoketonato ligands, which coordinate to rhodium(I) via (N,O) donors. The first complex of this type, (1-aminophenolato-N,O)dicarbonylrhodium(I) monohydrate, was prepared in 1985 [31]. The larger *trans* influence [32] of the nitrogen compared to oxygen is clearly distinguished from the rhodium-carbonyl bonds, which are longer when located *trans* to nitrogen. This study thus focuses on dicarbonyl rhodium(I) complexes containing aryl chloro derivatives [33] of 2-(phenylamino)pent-3-en-4-onate (PhonyH [34]), as model anionic N,O-bidentate ligands. It reports the effect of substitution of hydrogen by chloro on different positions of the phenyl ring in [Rh(Phony)$(CO)_2$] (**1**) type complexes with regard to packing modes, metal–metal interactions, potential chloro–chloro interactions, and other bonding distances and angles from solid-state data and theoretically optimized structures, and the evaluation of the reactivity towards iodomethane oxidative addition.

2. Experimental details

All reagents were used as purchased. The PhonyH N,O-bidentate ligands were prepared according to previously published methods [23, 24]. Preparation of $[Rh(Phony)(CO)_2]$ is reported as an example of a typical preparation method. $[Rh(\mu\text{-}Cl)(CO)_2]_2$ was prepared *in situ* by heating $RhCl_3 \cdot 3H_2O$ (0.105 g, 0.397 mM) in DMF (2 mL) under reflux for 30 min. PhonyH (0.0786 g, 0.449 mM, 1.14 eq) was added to the cooled DMF solution of $[RhCl(CO)_2]_2$ and the product was precipitated within 1 min by ice-water and obtained by centrifuge. Crystals suitable for X-ray diffraction were obtained from slow evaporation from a dichloromethane solution in 0.104 g (78.8%) yield. All dicarbonyl N,O-bidentate rhodium (I) complexes were prepared using the same procedure. The products are stable in air over a period of several months once water is removed. Spectroscopic data for the different complexes are given below, with numbering as shown in scheme 1.

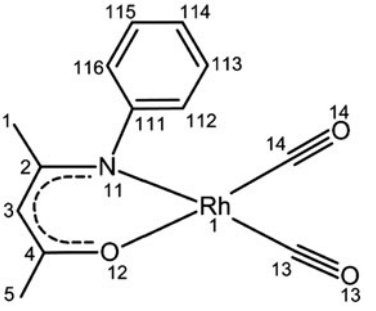

Scheme 1.

2.1. *[Rh(Phony)(CO)$_2$] (1)*

Yield: 0.0831 g (65.8%). IR (KBr): $\nu_{CO(asym)}$ 1999 (s) cm^{-1}; $\nu_{CO(sym)}$ 2062 (s) cm^{-1}. UV/Vis ($CHCl_3$): $\lambda_{max(1)} = 329$ nm, $\varepsilon_1 = 5102\ M^{-1}\ cm^{-1}$; $\lambda_{max(2)} = 265$ nm, $\varepsilon_2 = 6497\ M^{-1}\ cm^{-1}$. ^1H NMR (600.28 MHz, $CDCl_3$, 25 °C): 1.76 (s, 5H), 2.12 (s, 1H), 5.27 (s, 3H), 7.05 (d, 112; 116H), 7.17 (t, 114H), 7.34 (t, 113H; 115H). ^{13}C NMR (150.96 MHz, $CDCl_3$, 25 °C): 23.31 (s, 1C), 25.95 (s, 5C), 99.05 (s, 3C), 123.97 (s, 112C; 116C), 125.52 (s, 114C), 128.82 (s, 113C; 115C), 157.25 (s, 111C), 165.53 (s, 2C), 178.31 (s, 4C), 183.70 (d, 14C), 184.58 (d, 13C).

2.2. *[Rh(2'-Cl-Phony)(CO)$_2$] (2)*

Yield: 0.0714 g (51.4%). IR (KBr): $\nu_{CO(asym)}$ 2005 (s) cm^{-1}; $\nu_{CO(sym)}$ 2075 (s) cm^{-1}. UV/Vis ($CHCl_3$): $\lambda_{max(1)} = 329$ nm, $\varepsilon_1 = 8469\ M^{-1}\ cm^{-1}$; $\lambda_{max(2)} = 267$ nm, $\varepsilon_2 = 8479\ M^{-1}\ cm^{-1}$. ^1H NMR (600.28 MHz, $CDCl_3$, 25 °C): 1.73 (s, 5H), 2.13 (s, 1H), 5.33 (s, 3H), 6.15 (m, 114H; 116H), 7.28 (d, 113H), 7.44 (d, 115H). ^{13}C NMR (150.96 MHz, $CDCl_3$, 25 °C): 22.74 (s, 1C), 26.15 (s, 5C), 99.22 (s, 3C), 126.01 (s, 112C), 126.82 (s, 114C), 127.26 (s, 115C), 128.26 (s, 116C), 129.76 (s, 113C), 153.65 (s, 111C), 165.95 (s, 2C), 179.66 (s, 4C), 183.75 (d, 14C), 184.30 (d, 13C).

Table 1. Structural information on [Rh(XPhony)$(CO)_2$] complexes.

Compound	**1**	**2**	**3**	**4**	**5**[a]
Crystal color	Yellow	Yellow	Yellow	Colorless	Colorless
Crystal system	Monoclinic	Orthorhombic	Orthorhombic	Triclinic	Orthorhombic
Space group	*I2/a*	*Pbca*	*Pnma*	*P*$\bar{1}$	$P_2 1_2 1_2 1$
a (Å)	13.3756(2)	14.309(4)	13.163(2)	7.157(2)	7.8800(2)
b (Å)	9.2915(1)	10.085(3)	6.8055(9)	9.983(2)	12.3010(3)
c (Å)	21.2210(3)	18.886(6)	14.962(2)	10.654(3)	15.0740(3)
α (°)	90	90	90	83.086(1)	90
β (°)	96.193(1)	90	90	71.601(2)	90
γ (°)	90	90	90	82.059(1)	90
V (Å^3)	2621.94(6)	2725(1)	1340.2(3)	713.0(3)	1461.15(6)
Z	8	8	4	2	4
D_{Calcd} (Mg m^{-3})	1.688	1.3792	1.822	1.873	1.828
Crystal size (mm^3)	0.08 × 0.10 × 0.23	0.13 × 0.28 × 0.37	0.04 × 0.06 × 0.30	0.16 × 0.22 × 0.26	0.12 × 0.33 × 0.41
μ (mm^{-1})	1.301	1.451	1.475	1.576	1.538
Reflections measured	9457	53,966	12,246	17,679	37,505
unique, R_{int}	2854, 0.0268	3390, 0.0577	1579, 0.0706	3108, 0.0298	3632, 0.0390
Completeness to θ_{max}	99.5%	99.7%	99.6%	99.7%	100%
No. of parameters	165	174	105	171	183
GOF on F^2	1.010	1.081	1.293	1.076	0.963
R_1 [$I \geq 2\sigma(I)$]	0.0268	0.0296	0.0600	0.0211	0.0163
wR_2 (all data, F^2)	0.0516	0.0708	0.1377	0.0492	0.0363
$\Delta\rho$ min/max (e·Å^{-3})	−0.498/0.800	−0.539/1.294	−2.905/1.746	−0.951/0.872	−0.330/0.275

[a]Flack parameter for **5**: −0.01(2).

2.3. *[Rh(4'-Cl-Phony)(CO)$_2$] (3)*

Yield: 0.1023 g (70.1%). IR (KBr): $\nu_{CO(asym)}$ 1995 cm^{-1}; $\nu_{CO(sym)}$ 2065 (s) cm^{-1}. UV/Vis ($CHCl_3$): λ_{max} = 329 nm, ε = 6879 M^{-1} cm^{-1}. ^{1}H NMR (600.28 MHz, $CDCl_3$, 25 °C): 1.75 (s, 5H), 2.12 (s, 1H), 5.28 (s, 3H), 7.00 (d, 113H; 115H), 7.31 (d, 112H; 116H). ^{13}C NMR (150.96 MHz, $CDCl_3$, 25 °C): 23.40 (s, 1C), 26.01 (s, 5C), 99.22 (s, 3C), 125.44 (s, 113C; 115C), 128.94 (s, 112C; 116C), 131.04 (s, 111C), 155.66 (s, 114C), 165.62 (s, 2C), 179.03 (s, 4C), 183.80 (d, 14C), 184.33 (d, 13C).

2.4. *[Rh(2',4'-diCl-Phony)(CO)$_2$] (4)*

Yield: 0.0903 g (59.0%). IR (KBr): $\nu_{CO(asym)}$ 1990 (s) cm^{-1}; $\nu_{CO(sym)}$ 2069 (s) cm^{-1}. UV/Vis ($CHCl_3$): λ_{max} = 328 nm, ε = 12678 M^{-1} cm^{-1}. ^{1}H NMR (600.28 MHz, $CDCl_3$, 25 °C): 1.73 (s, 5H), 2.13 (s, 1H), 5.38 (s, 3H), 7.09 (d, 116H), 7.27 (dd, 115H), 7.46 (d, 113H). ^{13}C NMR (150.96 MHz, $CDCl_3$, 25 °C): 22.81 (s, 1C), 26.21 (s, 5C), 99.39 (s, 3C), 126.86 (s, 111C), 127.23 (s, 116C), 129.21 (s, 115C), 129.50 (s, 112C), 131.63 (s, 114C), 152.25 (s, 113C), 165.99 (s, 2C), 180.30 (s, 4C), 183.71 (d, 14C), 184.17 (d, 13C).

2.5. *[Rh(2',6'-diCl-Phony)(CO)$_2$] (5)*

Yield: 0.1270 g (83.4%). IR (KBr): $\nu_{CO(asym)}$ 2001 (s) cm^{-1}; $\nu_{CO(sym)}$ 2072 (s) cm^{-1}. UV/Vis ($CHCl_3$): $\lambda_{max(1)}$ = 327 nm, ε_1 = 9279 M^{-1} cm^{-1}; $\lambda_{max(2)}$ = 264 nm, ε_2 = 7818 M^{-1} cm^{-1}. ^{1}H NMR (600.28 MHz, $CDCl_3$, 25 °C): 1.70 (s, 5H), 2.015 (s, 1H), 5.38 (s, 3H), 7.10 (t, 114H), 7.40 (d, 113H; 115H). ^{13}C NMR (150.96 MHz, $CDCl_3$, 25 °C): 22.23 (s, 1C), 26.35 (s, 5C), 99.43 (s, 3C), 126.85 (s, 111H), 128.37 (s, 113C; 115C), 130.26 (s, 114C), 150.64 (s, 112C; 116C), 166.04 (s, 2C), 180.93 (s, 4C), 183.69 (d, 14C), 184.15 (d, 13C).

3. Analytical techniques

3.1. *Single-crystal X-ray crystallography*

The data collection for **1** was done on an Oxford Diffraction Xcalibur 3 Crysalis CCD system [35] using Mo Kα (0.71073 Å) radiation and ω-scans at 100(2) K. Intensity data were extracted and integrated using CrysAlis RED [36]. The data for **2–5** were collected on a Bruker Apex II 4 K CCD diffractometer using Mo *K*α (0.71073 Å) radiation and ω-scans at 100(2) K. All reflections for **2–5** were merged and integrated with SAINT-PLUS [37] and corrected for Lorentz, polarization, and absorption effects using SADABS [38]. All structures were solved by the heavy atom method and refined through full-matrix least-squares cycles using SHELX-97 [39] as part of the WinGX [40] package with $\Sigma(||F_o|-|F_c||)^2$ being minimized. All non-H atoms were refined with anisotropic displacement parameters, while hydrogens were constrained to parent atom sites using a riding model [aromatic C–H = 0.95 Å $\{U_{iso}(H) = 1.2U_{eq}\}$; aliphatic C–H = 0.98 Å $\{U_{iso}(H) = 1.5U_{eq}\}$]. The graphics were done with the DIAMOND visual crystal structure information system software [41]. The basic crystallographic data are reported in table 1.

3.2. *Computational data*

Optimization and energy calculations were obtained using the GAUSSIAN-03W [42] software package. DFT calculations were done at the B3LYP [43] level of theory with the

6-31G++(d,p) [44, 45] basis set for the main group elements and LanL2DZ [46] for rhodium, using the High Performance Computing Facility of the University of the Free State. Optimized structures were verified as minima through frequency analysis and from these data the unscaled stretching frequencies of the carbonyl groups were identified. Zero-point vibrational corrections have been applied, as well as corrections concerning differences in molecular composition.

3.3. *Nuclear magnetic resonance spectroscopy*

The ^{13}C and ^{1}H FT-NMR solution-state spectra were recorded at 150.96 and 600.28 MHz, respectively, on a Bruker AXS 600 MHz at 25 °C in $CDCl_3$; chemical shifts are reported in ppm relative to the solvent peaks with numbering schemes corresponding to scheme 1.

3.4. *Infrared spectroscopy*

FT-IR spectra were recorded on a Bruker Tensor 27 spectrophotometer from 4000 to 400 cm^{-1} as KBr pellets or as liquid samples in dry organic solvents (toluene or dichloromethane) in a NaCl cell (2350–1600 cm^{-1}) equipped with a temperature cell regulator accurate within 0.3 °C.

3.5. *UV/Vis spectroscopy*

All kinetic experiments were carried out in air and all solvents were predried over aluminum oxide and distilled. UV/Vis absorbance spectra were collected on a Varian Cary 50 Conc spectrophotometer in a 1.000 ± 0.001 cm quartz cuvette, which was equipped with a temperature cell regulator accurate within 0.1 °C.

Attempted iodomethane oxidative addition reactions, although known to proceed cleanly in rhodium(I) L,L′-Bid ligand systems [27], were unsuccessful over a period of 3–4 days, monitored by both UV/Vis and IR spectroscopy. Typical concentrations of iodomethane concentrations of up to 1 M, and $[Rh] = 10^{-4}-10^{-3}$ M, respectively, were monitored. Only slow decomposition reactions, neither attributable to the formation of rhodium(III) alkyl nor acyl species, were observed after approximately 100 h.

4. Results

The bidentate ligands react stoichiometrically (1 : 2) with $[Rh(\mu\text{-}Cl)(CO)_2]_2$ to yield [Rh(N,O-Bid)$(CO)_2$], where the mono-anionic N,O-bidentate ligands are Phony (**1**), 2′-Cl-Phony (**2**), 4′-Cl-Phony (**3**), 2′,4′-diCl-Phony (**4**), and 2′,6′-diCl-Phony (**5**), characterized by single-crystal X-ray crystallography (figure 1). All complexes are stable under ambient conditions. Table 1 contains the basic crystal data for structures of **1–5** with important geometrical parameters of the solid state summarized in table 2. Expanded fractions of the unit cells are only given for **1** and **5** and are shown in figure 2, illustrating some of the hydrogen interactions.

Complexes **2–4** all show similar behavior to **1** and are briefly discussed but are illustrated in Supplementary material. Similarly, packing for only **1** and **5** are shown in figure 3, illustrating in particular the Rh···Rh interactions. Again, **2–4** all show similar behavior to **1**

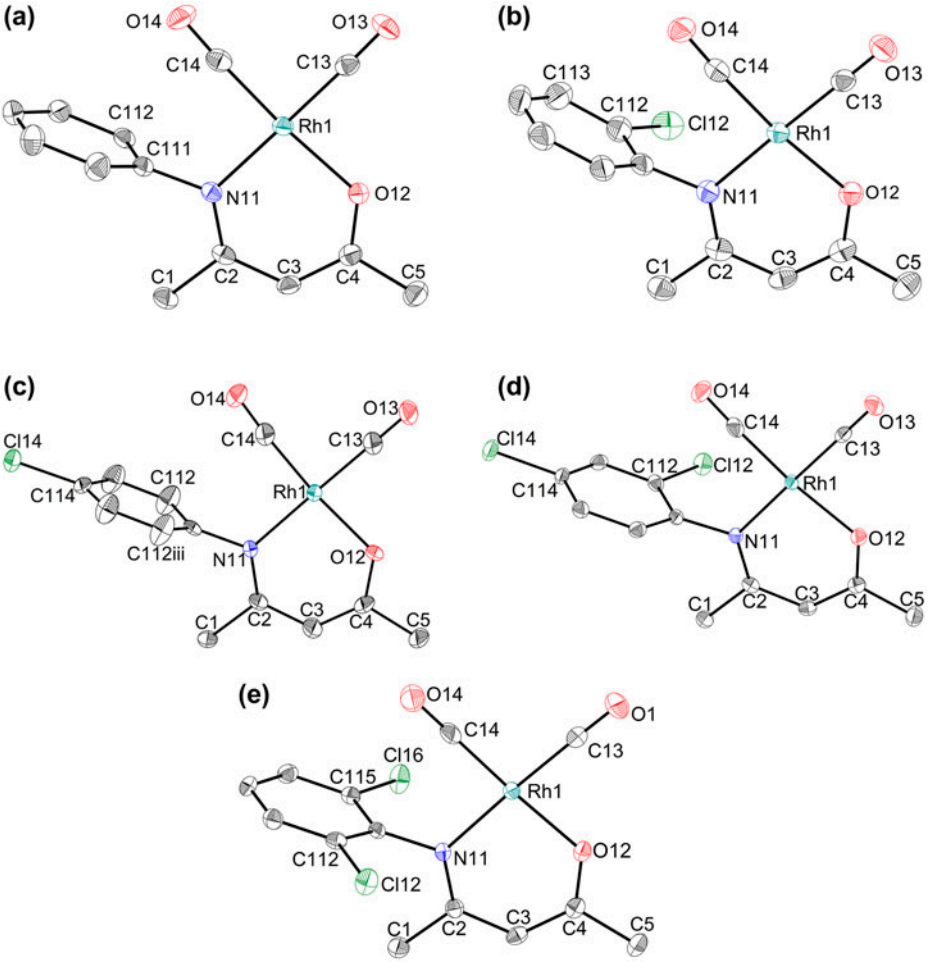

Figure 1. DIAMOND [41] views of (a) [Rh(Phony)$(CO)_2$] (**1**), (b) [Rh(2′-Cl-Phony)$(CO)_2$] (**2**), (c) [Rh(4′-Cl-Phony)$(CO)_2$] (**3**), (d) [Rh(2′,4′-diCl-Phony)$(CO)_2$] (**4**) and (e) [Rh(2′,6′-diCl-Phony)$(CO)_2$] (**5**) (50% probability displacement ellipsoids), where Phony = 2-(phenylamino)pent-3-en-4-onate. Hydrogens are omitted for clarity. For carbons in the phenyl ring, the first digit indicates molecule number, the second indicates ring number and the third indicates the position of the atom in the ring. Some labels have been omitted for clarity, but all rings are numbered in the same consistent way. For Cl, the first digit indicates molecule number while the second indicates the position on the phenyl ring. Symmetry operator for **3**: (iii) $x, -y+½, z$.

and are being briefly discussed but illustrated in Supplementary material. It is clear that **5** behaves differently than **1**–**4**, as highlighted further below.

Solid-state data and computational results as obtained from DFT calculations are correlated in tables 2 and 3 and are visually illustrated in figure 4. Comparison to similar complexes reported in literature is presented in table 4. The relative values for the energies which were obtained from DFT calculations are presented in figure 5 and reported in table 5. Included are both the optimizations of the free PhonyH as well as the [Rh(Phony)$(CO)_2$] and the chloro derivatives thereof. This is further discussed below, but is also manifested by the good agreement between the energies obtained from the DFT optimized structures *versus* that of the corresponding single-point energies calculated using the solid-state structure

Table 2. Comparison of selected geometrical parameters of solid-state structures of **1–5** with their corresponding optimized counterparts (Å, °).

	1		**2**		**3**		**4**		**5**	
Atoms	Solid state	DFT	Solid state	DFT	Solid state	DFT	Solid state	DFT	Solid state	DFT
Rh_1–N_{11} (Å)	2.058(2)	2.105	2.054(2)	2.107	2.065(8)	2.104	2.020(1)	2.107	2.051(1)	2.112
Rh_1–O_{12} (Å)	2.032(2)	2.064	2.019(2)	2.064	2.033(6)	2.064	2.057(2)	2.064	2.017(1)	2.065
Rh_1–C_{13} (Å)	1.866(2)	1.900	1.858(3)	1.899	1.86(1)	1.900	1.873(2)	1.900	1.872(2)	1.898
Rh_1–C_{14} (Å)	1.841(3)	1.874	1.849(3)	1.873	1.84(1)	1.874	1. 838(2)	1.872	1.834(2)	1.871
C_{13}–O_{13} (Å)	1.142(3)	1.140	1.135(4)	1.140	1.14(1)	1.140	1.133(2)	1.139	1.134(2)	1.140
C_{14}–O_{14} (Å)	1.143(3)	1.144	1.143(3)	1.143	1.15(1)	1.143	1.142(2)	1.143	1.140(3)	1.143
$N_{11}\cdots O_{12}$ (Å)	2.906(2)	2.940	2.882(3)	2.940	2.93(1)	2.939	2.893(2)	2.939	2.880(2)	2.940
Rh displacement[a] (Å)	0.0218(2)	0.000	0.0266(2)	0.004	0	0	0.0206(2)	0.003	0.0089(1)	0.0002
N_{11}–Rh_1–O_{12} (°)	90.55(6)	89.75	90.08(8)	89.63	91.2(3)	89.70	90.36(5)	89.56	90.15(6)	89.48
O_{12}–Rh_1–C_{13} (°)	89.75(8)	86.58	88.5(1)	86.59	87.9(4)	86.56	88.76(6)	86.63	87.63(7)	86.65
C_{13}–Rh_1–C_{14} (°)	86.5(1)	89.39	87.2(1)	89.41	87.0(5)	89.41	87.07(8)	89.38	89.45(9)	89.37
N_{11}–Rh_1–C_{14} (°)	93.13(9)	94.28	94.2(1)	94.38	94.0(4)	94.33	93.81(7)	94.43	92.77(8)	94.50
N_{11}–$C_2\cdots C_4$–O_{12} (°)	−0.4(2)	0.30	1.4(1)	0.17	0.0(7)	0.02	−0.7(1)	0.11	3.7(2)	−0.01
Dihedral angle[b] (°)	87.88(8)	89.99	85.20(9)	86.74	90.0(2)	89.95	85.85(6)	87.06	89.35(7)	89.99

[a]Displacement of the Rh atom from the N_{11}–O_{12}–C_{13}–C_{14} coordination plane (see figure 1).
[b]Dihedral angle defined as that between the N_{11}–C_2–C_3–C_4–O_{12} plane and the N-substituted phenyl ring.

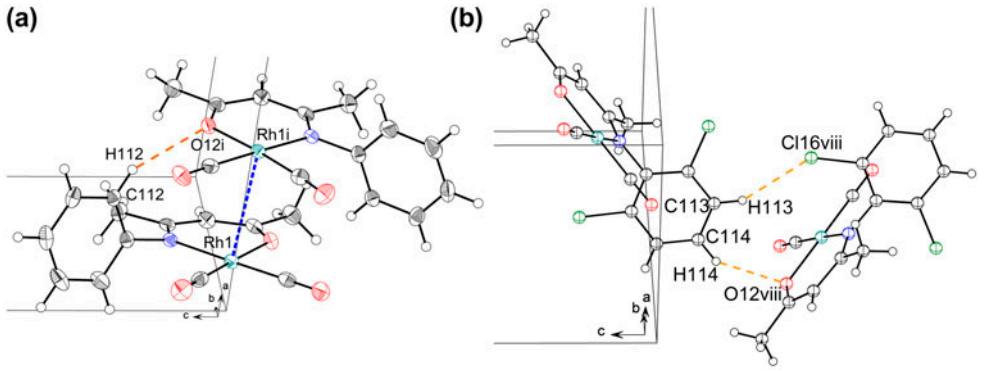

Figure 2. Partial unit cell for (a) **1** and (b) **5** with the intermolecular hydrogen bonding interaction indicated with a dashed line and the intermolecular rhodium···rhodium interaction by a dotted line. Symmetry operators: (i) $-x+\frac{1}{2}, y, -z$; (viii) $-x+1\frac{1}{2}, -y+2, z+\frac{1}{2}$.

geometries (table 5). The energy values listed are relative values to the compounds with the lowest energies for the PhonyH and [Rh(Phony)$(CO)_2$] as separate groups, respectively.

5. Discussion

Significant hydrogen interactions are present in all complexes except **2** and play an important role in the packing of these compounds, along with intermolecular rhodium···rhodium interactions, also present in all complexes except **5**. Disorders of the hydrogens on the methyl groups in these complexes have been observed in **3**. Although the complexes are chemically similar, packing is influenced by different contributing factors. The intermolecular hydrogen interactions are evident in **1**, along with a rhodium···rhodium interaction, while the absence of Rh···Rh in **5** is clear (see figures 2(a), (b), and 3(a), (b), respectively).

In **1**, Rh_1 is displaced from the plane formed by N_{11}, O_{12}, C_{13}, and C_{14} by 0.0218(2) Å. The distance between Rh_1 and Rh_1^{i} is 3.4358(2) Å and the dihedral angle between the N_{11}–O_{12}–C_{13}–C_{14} plane and the rhodium···rhodium interaction is 83.14(4)°.

The introduction of an additional potential hydrogen bonding atom in the form of a chloro at the 2′-position on the phenyl ring [figure 1(b) in **2**] does not result in significant hydrogen interaction; instead, the packing style is still characterized by intermolecular rhodium···rhodium interactions (see figure S2(a), see online supplemental material at http://dx.doi.org/10.1080/00958972.2013.878801). The complex therefore exhibits crystallographic "dimerism" instead of polymerism, in contrast to **4** (which has a chloro in the *ortho* position on the phenyl ring as well). Rh_1 is displaced from the plane formed by N_{11}, O_{12}, C_{13}, and C_{14} by 0.0266(2) Å. The distance between Rh_1 and Rh_1^{ii} in **2** is 3.4151(7) Å and the angle between the N_{11}–O_{12}–C_{13}–C_{14} plane with the rhodium···rhodium interaction is 78.44(4)°.

Complex **3** exhibits intermolecular interactions to two different independent molecules, of which one is an oxygen–hydrogen interaction (figure S2(b)). The other is a medium Rh···Rh interaction, with the distance between Rh_1 and Rh_1^{v} of 3.5477(5) Å. The angle between the N_{11}–O_{12}–C_{13}–C_{14} plane and the Rh···Rh interaction is 73.56(2)°.

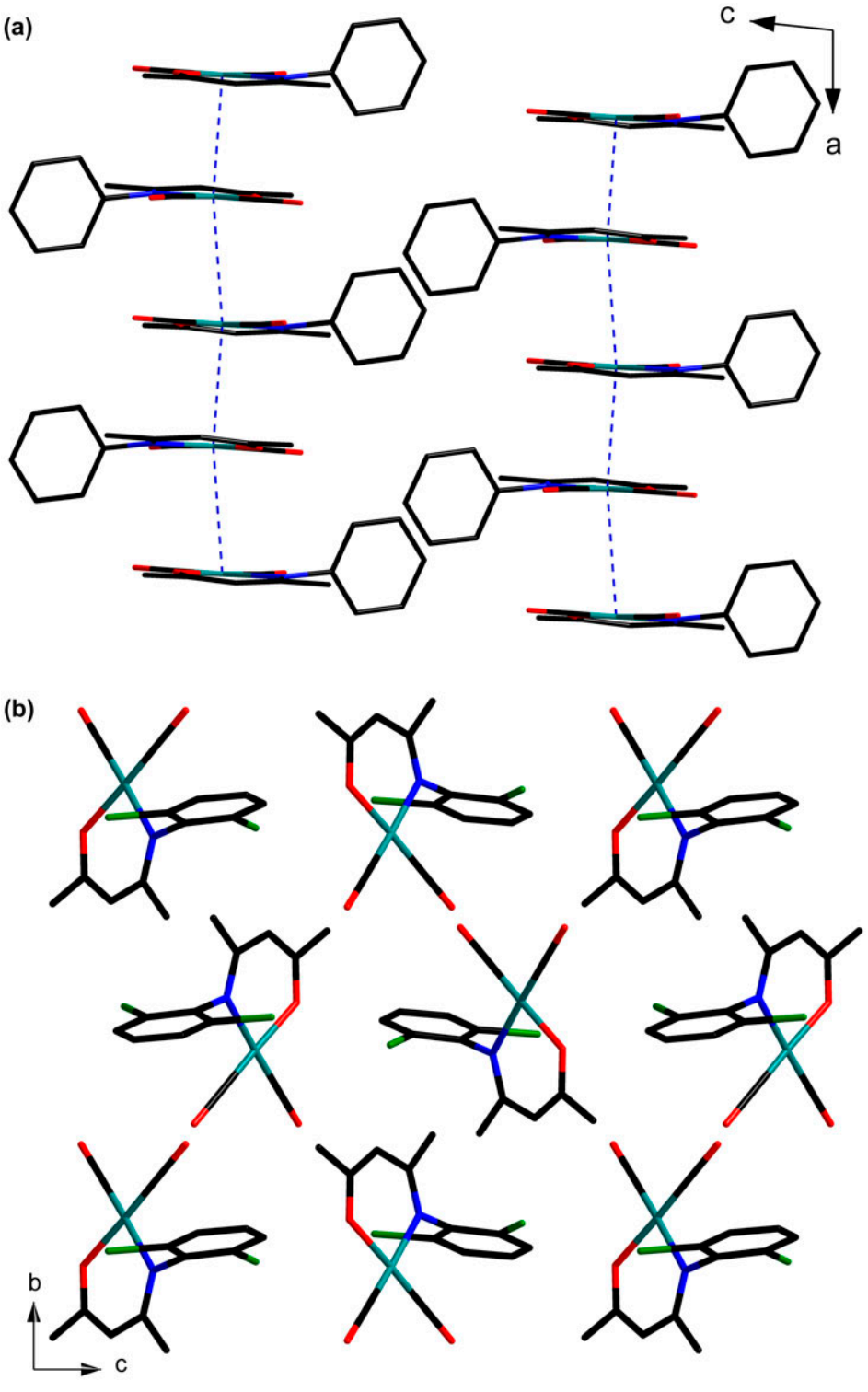

Figure 3. Packing diagram of (a) **1** viewed along the *b*-axis and (b) **5** viewed along the *a*-axis.

Table 3. Observed solid state and calculated ν_{CO} data for the Phony type complexes, [Rh(N,O-Bid)$(CO)_2$].

	$\nu_{CO(asym)}$ (cm^{-1})		$\nu_{CO(sym)}$ (cm^{-1})	
Compound	Observed (solid state)	Calculated	Observed (solid state)	Calculated
1	1999	2001	2062	2056
2	2005	2001	2075	2057
3	1995	2001	2065	2057
4	1990	2002	2069	2058
5	2001	2001	2072	2058

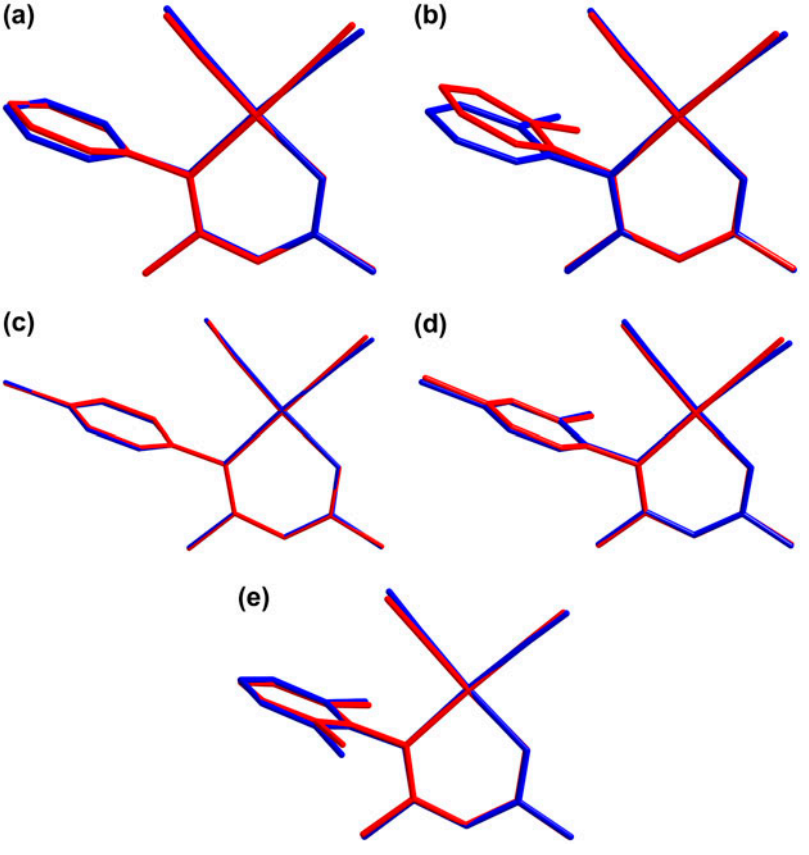

Figure 4. Overlay figures of the calculated (DFT) and solid-state structures of (a) [Rh(Phony)$(CO)_2$], RMS value = 0.163 Å; (b) [Rh(2′-Cl-Phony)$(CO)_2$], RMS value = 0.233 Å; (c) [Rh(4′-Cl-Phony)$(CO)_2$], RMS value = 0.062 Å; (d) [Rh(2′,4′-diCl-Phony)$(CO)_2$], RMS value = 0.088 Å; and (e) [Rh(2′,6′-diCl-Phony)$(CO)_2$], RMS value = 0.126 Å. Overlay fit includes all non-hydrogen atoms. The blue structures denote the calculated complexes, while the red structures refer to the observed solid-state complexes reported in table 1.

Intermolecular hydrogen interactions are evident in **4**, along with a rhodium···rhodium interaction (see figure S2(c)). Rh_1 is displaced from the plane formed by N_{11}, O_{12}, C_{13}, and C_{14} by a distance of 0.0068(2) Å. The distance between Rh_1 and $Rh_1{}^{vi}$ is 3.5836(9) Å and the angle between the N_{11}–O_{12}–C_{13}–C_{14} plane and the Rh···Rh interaction is 72.46(3)°.

Table 4. Comparison of **1–5** with other [Rh(L,L′-Bid)$(CO)_2$] complexes, with L,L-Bid indicating ligands with L, L′ = N,O- or O,O′-sets of donor atoms.

CSD [9] reference code[a]	Packing style[b]	d(N···O)[f] (Å)	N_{11}–Rh–O_{12}[c] (°)	N_{11}–C_2–C_4–O_{12}[f] (°)	d(Rh···Rh) (Å)	Reference
DEXHUJ (**1**)	HT	2.771(5)	86.8(1)	1.4(4)	3.332(2)	[47]
KEFJUB (**2**)	O	2.809(6)	88.8(2)	−1.0(5)	N/A	[48]
KEFJOV (**3**)	HT	2.831(2)	89.00(7)	0.7(2)	3.2337(4)	[48]
BTFARH (**4**)	D	2.8583(0)	89.751(0)	1.692(0)	3.5368(0)	[49]
QUNBAC (**5**)	HT	2.869(4)	89.5(1)	1.2(4)	3.402(3)	[50]
5	O	2.880(2)	90.15(6)	3.7(2)	N/A	
2	HT	2.882(3)	90.08(8)	1.4(1)	3.4151(7)	
KAKYUR (**6**)	D	2.887(8)	90.1(3)	1.0(8)	3.346(1)	[51]
VAVJUX (**7**)	D	2.89(7)	90.6(4)	2(1)	3.315(1)	[52]
4	HT	2.893(2)	90.36(5)	−0.7(1)	3.5836(9)	
1	HT	2.906(2)	90.55(6)	−0.4(2)	3.4358(2)	
ACABRH02 (**8**)	HT	2.9089(4)	90.827(6)	0.12(1)	3.2533(3)	[53]
3	HT	2.93(1)	91.2(3)	0.0(7)	3.5477(5)	
BUPCUK (**9**)	HT	2.9960(8)	92.58(1)	26.48(3)[d]	3.3517(7)	[54]
Average		2.88(7)	90.0(6)	1(2)[e]	3.396(4)	

[a]DEXHUJ = (1*RS*, 4*SR*)-(trifluoroacetyl-menthonato-O,O′) dicarbonylrhodium(I); KEFJUB = dicarbonyl (9-oxyphenalen-1-one-O, O′)rhodium(I); KEFJOV = dicarbonyl(5-methyl-9-oxyphenalen-1-one-O,O′)rhodium(I); BTFARH = benzoyl-1,1,1-trifluoroacetonatodicarbonylrhodium(I); QUNBAC = dicarbonyl(4-amino-1,1,1-trifluoro-3-penten-2-onato-N,O)rhodium(I); KAKYUR = dicarbonyl (1-ferrocenyl-4,4,4-trifluoro-1,3-butanedionato)rhodium(I); VAVJUX = tetracarbonyl(μ2-3,3′-hexafluoro-glutarylbis-(1*R*)-camphorato-O,O′,O″,O‴)dirhodium(I); ACABRH02 = acetylacetonatodicarbonyl-rhodium(I); BUPCUK = dicarbonyl-(1*S*)-3-trifluoroacetyl-camphoraterhodium(I) dicarbonyl-(1*R*)-3-trifluoroacetylcamphorateiridium(I).
[b]HT: head-to-tail; HH: head-to-head; D: diagonal; O: other.
[c]Average values are used for complexes with more than one independent molecule in the asymmetric unit.
[d]Torsion angle excluded in the calculation of the average value due to outlier nature.
[e]Average calculated for absolute values of angles.

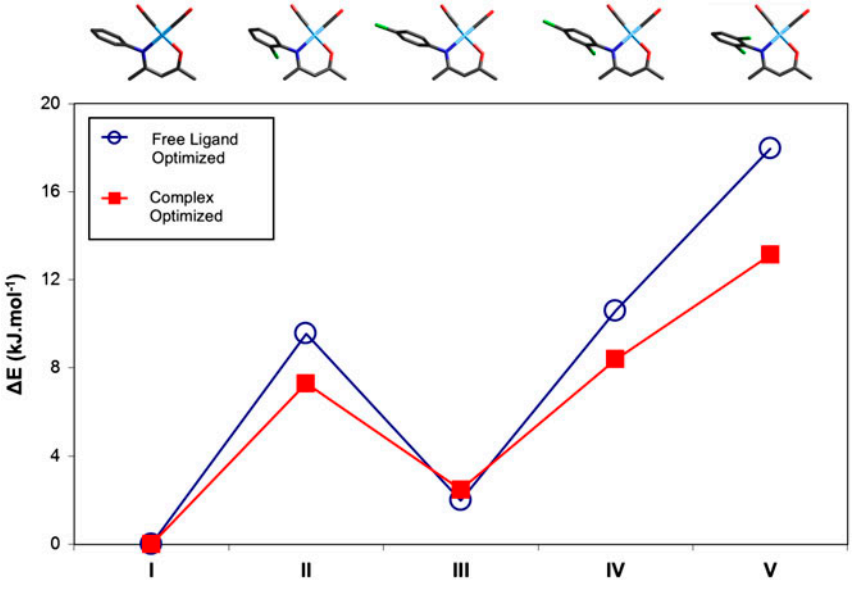

Figure 5. Diagram of calculated optimized relative energies of free N,O-BidH (blue [33]) and [Rh(N,O-Bid)$(CO)_2$] complexes (red) from GAUSSIAN-03W [42]. (see http://dx.doi.org/10.1080/00958972.2013.878801 for color version).

Table 5. Optimized and single-point (solid-state data) calculated energies of N,O-BidH compounds and complexes of the type [Rh(N,O-Bid)$(CO)_2$].

	N,O-BidH compounds				[Rh(N,O-Bid)$(CO)_2$] complexes			
N,O-bidentate ligand	ΔE_{opt} [a] (Hartree)	ΔE_{opt} [a] (kJ M^{-1})	ΔE_{sp} [b] (Hartree)	ΔE_{sp} [b] (kJ M^{-1})	ΔE_{opt} [c] (Hartree)	ΔE_{opt} [c] (kJ M^{-1})	ΔE_{sp} [d] (Hartree)	ΔE_{sp} [d] (kJ M^{-1})
Phony	0.00000	0.0	0.0697	183	0.0000	0.0	0.0290	76.1
2′-Cl-Phony	0.00364	9.6	0.0428	112	0.00278	7.3	0.0189	49.6
4′-Cl-Phony	0.00076	2.0	0.0854	224[e]	0.00094	2.5	0.0190	50.0
2′,4′-diCl-Phony	0.00404	10.6	0.0118	31[f]	0.00320	8.4	0.0000	0.0
2′,6′-diCl-Phony	0.00684	18.0	0.0602	158	0.00500	13.1	0.0033	8.8

[a]Optimized and corrected energy; relative to PhonyH = 0.
[b]Single-point energy (based on solid-state geometry); relative to PhonyH = 0.
[c]Optimized and corrected energy; relative to [Rh(Phony)$(CO)_2$] = 0.
[d]Single-point energy (based on solid-state geometry); relative to [Rh(2′,4′-diClPhony)$(CO)_2$] = 0.
[e]Four independent molecules in the asymmetric unit.
[f]Two independent molecules in the asymmetric unit.

Care should be taken not to assign a chloro···chloro interaction to $Cl_{14}\cdots Cl_{12}^{vii}$ which displays a distance of 3.963(1) Å, since the possibility of such an interaction is refuted by the C–Cl···Cl angles of 144.29(6) and 92.19(7)°, which do not agree to one of the types assigned in the literature [7, 8]. Packing diagrams for **1** and **5** are illustrated in figure 3(a) and (b).

The crystal-packing diagrams of **1** and **3** reveal 1-D "coordination polymers," while **2** and **4** display dimerism (see figure 3 and Supplementary material). Complexes **1–4** exhibit clear Rh···Rh interactions. Packing occurs in a head-to-tail fashion with regard to the carbonyl groups for **1–4**, which is consistent with the literature, where the majority of rhodium L,L′-bidentate dicarbonyl complexes pack this way (table 4). Complex **5** is, however, the exception to this rule. Thus, no dz^2 Rh···Rh interaction was observed in **5**, although intermolecular hydrogen interactions are present [figure 3(b)]. Rh_1 is displaced from the plane formed by N_{11}, O_{12}, C_{13}, and C_{14} by a distance of 0.0987(1) Å. The absence of Rh···Rh interactions in **5** is attributed to steric intervention of the two chloro substituents on the phenyl ring of the 2,6-diCl-Phony moiety. The packing of the complex is therefore governed by both C–H···O and C–H···Cl interactions.

Overall, it turned out that Cl···Cl interactions are not that important in these systems, where the Rh···Rh interactions dominate. As soon as the Rh···Rh interactions are inhibited, the weak Cl interaction becomes more important. The Rh···Rh interactions (with distances of 3.4358(2) Å for **1**, 3.4151(7) Å for **2**, 3.5477(5) Å for **3,** and 3.5836(9) Å for **4**, respectively) indicate that there is a tendency for these distances to increase as the number of substituents on the phenyl ring increases.

Examples of crystal structures of complexes of the type [Rh(N,O-Bid)$(CO)_2$] in the literature are surprisingly limited [9]; a few complexes employ diketonato ligands (table 4). Upon coordination of the bidentate ligand, the unsaturated carbon–carbon bond of the pentenone backbone becomes delocalized and C_2–C_3 and C_3–C_4 distances no longer vary significantly. The N_{11}–$C_2\cdots C_4$–O_{12} torsion angles seem to be fairly independent of the electronic properties of chloro substituents on the ligand and do not follow a clear trend when compared with the N_{11}–Rh–O_{12} bite angles, displaying angles of less than 2° with the exception of **5** and **9**. In both these cases, the steric bulk of the ligand has a significant influence on the distortion of the N_{11}–C_2–C_3–C_4–O_{12} backbone of the ligand.

All the complexes adopt distorted square planar geometries, with the largest distortion of the rhodium from the N_{11}–O_{12}–C_{13}–C_{14} plane of 0.0987(1) Å for **5**, while the second largest is 0.0298(8) Å (**6**). While the N_{11}–Rh–O_{12} bite angles appear to be larger when rhodium is coordinated to more electron-donating ligands, the steric properties of the ligands also play an important role in the geometric parameters of such complexes. The Rh_1–C_{13} and Rh_1–C_{14} distances observed in the current study do not vary significantly in complexes with O,O-bidentate ligands; however, in complexes containing N,O-bidentate ligands an elongation of the Rh_1–C_{13} distances is clear and attributed to the larger *trans* influence of nitrogen.

Overlay diagrams visually comparing the theoretically optimized complexes with their experimental solid-state counterparts are shown in figure 4. Observed solid state (KBr) and calculated carbonyl stretching frequencies (ν_{CO}) for **1–5** are reported in table 3, showing a good correlation. The differences in the Rh_1–C_{13} and Rh_1–C_{14} distances are reflected in the CO stretching frequencies (ν_{CO}, see table 3), where the complex with the smallest difference between Rh_1–C_{13} and Rh_1–C_{14} (**2**, with d(Rh_1–C_{13}) and d(Rh_1–C_{14}) values of 1.858(3) Å and 1.849(3) Å, respectively) displays the highest CO stretching frequencies, suggesting the least efficient d–π^* interaction of the metal center with the carbonyl ligands. Similarly, the complex with the largest differences (**4**, with d(Rh_1–C_{13}) and d(Rh_1–C_{14}) values of 1.873 (2) Å and 1.838(2) Å, respectively) exhibit the lowest ν_{CO} values.

The solid-state structures of **1–5** show good correlation with the calculated (DFT) ones, with RMS overlay values ranging from 0.664 to 0.713 Å. Angles and distances are compared in table 2. The calculated energy (figure 5) of **5** is significantly larger than **1**–**4**, with **1** having the lowest energy. Although **2** and **3**, and **4** and **5** have identical chemical formulas, the differences in energy underline the influence of relative steric and electronic factors on the geometries. Despite the low RMS values, angles and distances vary significantly between the solid state and calculated structures. The Rh_1–N_{11} distances for **3** differ by 0.036 Å between the solid state and calculated structures, while the corresponding distances differ by as much as 0.087 Å in **4**. The differences in the Rh_1–O_{12} distances provide a contrast with the Rh_1–N_{11} distances since the complex with the most significant discrepancy between the Rh_1–N_{11} distances, **4**, only differs by 0.007 Å for Rh_1–O_{12}. The largest difference in Rh_1–O_{12} distances is observed in **5**, with a difference of 0.048 Å. While both the Rh_1–C_{13} and Rh_1–C_{14} distances show differences of 0.041 Å for **2** and 0.037 Å for **5** for the respective distances, the C_{13}–O_{13} and C_{14}–O_{14} distances show no significant difference between the solid state and calculated structures.

The observed differences between solid state and calculated structures are further underlined by the angles of the Rh polyhedra, with the *differences* being consistently largest for **1** : 0.80° for N_{11}–Rh_1–O_{12}, 3.17° for O_{12}–Rh_1–C_{13}, and 2.9° for C_{13}–Rh_1–C_{14}. An exception is the angle N_{11}–Rh_1–C_{14} where the largest difference of 1.73° in **5** is observed. The impact of packing effects and intermolecular bonds on the geometrical parameters of the solid-state structure, as previously discussed, is also reflected in the calculated energies for the optimized and solid-state structures. The dihedral angles between the N_{11}–C_2–C_3–C_4–O_{12} plane and the phenyl ring for *all* the complexes, both solid state and calculated, generally approaches 90° as a result of steric interference from the metal and carbonyl groups. This is in contrast with previous studies regarding the free ligands, PhonyH [34], and the derivatives thereof [23], where dihedral angles were as small as 38.36(9)° [33]. Following coordination, the degrees of freedom of the phenyl ring are decreased, stabilizing on approximately orthogonal to the enaminato N_{11}–C_2–C_3–C_4–O_{12} plane.

The relative energies of the different N,O-BidH compounds as uncoordinated, neutral ligands [33] as determined and optimized through DFT calculations are illustrated in figure 5, with the data given in table 5, and are compared with the relative energies of the corresponding [Rh(N,O-Bid)$(CO)_2$] complexes. Energies are relative to the compound with the lowest energy, which is [Rh(Phony)$(CO)_2$] (red) and PhonyH (blue) for the optimized free ligands. It is clear that the same trend is followed for the free ligands and the dicarbonyl complexes, indicating that the relative energies depend to a large extent on the chloro-substitution on the ligand phenyl ring.

The difference between the lowest and highest optimized energies, **1** and **5**, respectively, is 13.1 kJ M^{-1} (figure 5 and table 5). The calculated energies of the *ortho*-substituted **2** and *para*-substituted **3** differ from the energy of **1** by 7.3 kJ M^{-1} and 2.5 kJ M^{-1}, respectively, while the difference between **1, 4,** and **5** are, respectively, 8.4 kJ M^{-1} and 13.1 kJ M^{-1}. Complex **4** may be described as a combination of *ortho*- and *para*-substituted (**2** and **3**) while **5** is similar to two *ortho*-substituted complexes. The calculated optimized energies of **4** and **5** of 8.4 and 13.1 kJ M^{-1} roughly resemble the relative energies of **2** and **3** when added in this fashion: the energy of *ortho*-substituted **2** added to *para*-substituted **3**, simulating **4**, is 9.8 kJ M^{-1} while twice the energy of *ortho*-substituted **2** is 14.6 kJ M^{-1} and simulates **5**. The similarities between the energies accentuate the cumulative nature of the energies with respect to the position of the chloro substituents on the phenyl moiety. Further studies are being conducted to clarify whether this phenomenon is repeated in systems incorporating other substituents. The relative energy differences between complexes **1**–**5** follow the same trend as the relative energy differences for the uncoordinated ligands [25] which also display a cumulative nature.

The agreement between the calculated and single-point energies for the dicarbonyl complexes in particular, is remarkable. It is less true for the free ligands, in particular 4′-Cl-PhonyH, where the single-point energy differs by more than 200 kJ M^{-1} from the DFT optimized structure. Since the 4′-Cl-PhonyH solid-state structure, however exhibits four independent molecules in the asymmetric unit, it is assumed that the apparent high energy solid state isomers are significantly stabilized in these geometries by hydrogen bonding.

The dicarbonyl complexes reported here are good candidates to evaluate for reactivity by classic oxidative addition reactions. Attempted iodomethane oxidative addition reactions, although known to proceed cleanly in rhodium(I) L,L′-Bid ligand systems [55–58] were unsuccessful even after a few days, as monitored by both UV/Vis and IR spectroscopy. This was attributed to the significant steric effect induced at the rhodium(I) centers. Two carbonyl ligands also act as significant electron-withdrawing groups, further decreasing the electron density on the Rh(I) and rendering it even more unreactive towards oxidative addition. Only slow decomposition reactions, neither attributable to the formation of rhodium (III) alkyl nor acyl species, were observed after approximately 100 h. Thus, the effective "blocking" of the rhodium metal center was confirmed by these sterically hindered chlorinated enaminoketonato ligand systems.

6. Conclusion

Slight differences were observed in bond distances and angles between the separate complexes, confirmed through both X-ray diffraction and NMR techniques. The *trans* influence of nitrogen was confirmed through the elongation of the Rh_1–C_{13} bond compared to the

Rh_1–C_{14} bond. The contribution of chloro functionalities on the geometrical parameters are observed in the differences in Rh_1–C_{13} and Rh_1–C_{14} distances. This is supported by information from the calculated structures and literature, where the electronic properties of substituents on the phenyl ring impact the geometrical parameters of the respective complexes. This allows for tailoring of [Rh(N,O-Bid)$(CO)_2$] complexes to suit different criteria for utilization as possible catalysts. The calculated IR stretching frequencies, as seen in table 3, differ significantly from the observed solid-state stretching frequencies, supporting the postulated influence of different chloro substitutions on packing modes and bond lengths, where seemingly small differences in substitution cause large variations in packing modes. No significant difference between stretching frequencies for the calculated complexes **1–5** were, however, observed, and the significant differences between stretching frequencies of the solid-state complexes can be explained by the influences of intra- and intermolecular hydrogen, rhodium···rhodium, and π–π interactions on the packing. The position of the chlorine on the ring, and the subsequent influence on the packing modes, is also clearly signified in the variation in crystal systems and space groups as the position and number of the chlorines on the phenyl ring changes. Of structural interest is the fact that the phenyl ring of the bidentate enaminoketonato upon coordination adjusts its rotation to approximately 90° (as defined by the dihedral angle) without exception, whereas in the free form, the rotation as observed from the dihedral angle can be as little as *ca*. 38°. A fairly constant steric influence on the rhodium(I) is therefore to be expected. Further studies are thus being conducted to compare the impact of different halide substituents on general geometrical parameters as manifested in the steric hindrance around the metal center, as well as the cumulative effect of the energy in such complexes. It should also be noted that minimal Cl···Cl interactions were observed, and that Rh···Rh interactions dominated. Finally, the significant steric effect induced at Rh(I) is manifested by the inability to undergo classic iodomethane oxidative addition, confirming the significant stability towards oxidation by molecular oxygen, rendering these Rh(I) complexes extremely stable in air for extended periods of time.

Acknowledgments

Financial assistance from the University of the Free State is gratefully acknowledged, while Mr Leo Kirsten and Dr Inus Janse van Rensburg are thanked for the XRD data collections. We also express our gratitude to SASOL, the South African National Research Foundation (SA-NRF/THRIP), the University of the Free State Strategic Academic Cluster Initiative (Materials and Nanosciences), the Inkaba yeAfrica initiative, and the Swedish International Development Cooperation Agency (SIDA) for financial support of this project. Part of this material is based on work supported by the SA-NRF/THRIP under [grant number GUN 2068915]. Opinions, findings, conclusions, or recommendations expressed in this material are those of the authors and do not necessarily reflect the views of the SA-NRF.

Supplementary material

CCDC 742590–742594 contains the supplementary crystallographic data for this article. These data can be obtained free of charge from The Cambridge Crystallographic Data Center via www.ccdc.cam.ac.uk/data_request/cif.

References

[1] G.M.J. Schmidt. *Pure Appl. Chem.*, **27**, 647 (1971).
[2] I. Csöregh, T. Brehmer, P. Bombicz, E. Weber. *Cryst. Eng.*, **4**, 343 (2001).
[3] B.S. Green, G.M.J. Schmidt. *Israel Chemical Society Annual Meeting Abstracts*, 197 (1971).
[4] M.D. Cohen, G.M.J. Schmidt, F.I. Sonntag. *J. Chem. Soc.*, 2000 (1964).
[5] G.M.J. Schmidt. *J. Chem. Soc.*, 2014 (1964).
[6] G.R. Desiraju. *Crystal Engineering: The Design of Organic Solids*, Elsevier, Amsterdam (1989).
[7] G.R. Desiraju, R. Parthasarathy. *J. Am. Chem. Soc.*, **111**, 8725 (1989).
[8] F.F. Awwadi, R.D. Willett, K.A. Peterson, B. Twamley. *Chem. Eur. J.*, **12**, 8952 (2006).
[9] F.H. Allen. *Acta Crystallogr. Sect. C.*, **58**, 380 (2002).
[10] F. Zordan, L. Brammer, P. Sherwood. *J. Am. Chem. Soc.*, **127**, 5979 (2005).
[11] P.W.M.N. Van Leeuwen. *Homogeneous Catalysis, Understanding the Art*, Kluwer Academic Publishers, Dordrecht (2004).
[12] A.M. Trzeciak, J.J. Ziółkowski. *J. Organomet. Chem.*, **464**, 107 (1994).
[13] A. Van Rooy, E.N. Orij, P.G.J. Kamer, P.W.M.N. Van Leeuwen. *Organometallics*, **14**, 34 (1995).
[14] N.A. Bailey, E. Coates, G.B. Robertson, F. Bonati, R. Ugo. *Chem. Commun.*, 1041 (1967).
[15] R. Crous, M. Datt, D. Foster, L. Bennie, C. Steenkamp, J. Huyser, L. Kirsten, G. Steyl, A. Roodt. *Dalton Trans.*, 1108 (2005).
[16] A.C. Ferreira, R. Crous, L. Bennie, A.M.M. Meij, K. Blann, B.C.B. Bezuidenhoudt, D.A. Young, M.J. Green, A. Roodt. *Angew. Chem. Int. Ed.*, **46**, 2273 (2007).
[17] G. Steyl, A. Roodt. *S. Afr. J. Chem.*, **59**, 21 (2006).
[18] W. Purcell, S.S. Basson, J.G. Leipoldt, A. Roodt, H. Preston. *Inorg. Chim. Acta*, **234**, 153 (1995).
[19] G.J.S. Venter, G. Steyl, A. Roodt. *Acta Crystallogr.*, **E65**, m1606 (2009).
[20] J.A. Viljoen, H.G. Visser, A. Roodt. *Acta Crystallogr.*, **E66**, m603 (2010).
[21] L. Herbst, R. Koen, A. Roodt, H.G. Visser. *Acta Crystallogr.*, **E66**, m801 (2010).
[22] G. Steyl, A. Roodt. *S. Afr. J. Chem.*, **59**, 21 (2006).
[23] G. Steyl, G.J. Kruger, A. Roodt. *Acta Crystallogr.*, **C60**, m473 (2004).
[24] C. Sacht, M.S. Datt, S. Otto, A. Roodt. *J. Chem. Soc., Dalton Trans.*, 4579 (2000).
[25] M. Schutte, G. Kemp, H.G. Visser, A. Roodt. *Inorg. Chem.*, **50**, 12486 (2011).
[26] A. Brink, H.G. Visser, A. Roodt. *J. Coord. Chem.*, **64**, 122 (2011).
[27] A. Roodt, H.G. Visser, A. Brink. *Crystallogr. Rev.*, **17**, 241 (2011).
[28] H.J. van der Westhuizen, R. Meijboom, M. Schutte, A. Roodt. *Inorg. Chem.*, **49**, 9599 (2010).
[29] C.G. Pitt, L.K. Monteith, L.F. Ballard, J.P. Collman, J.C. Morrow, W.R. Roper, D. Ulkü. *J. Am. Chem. Soc.*, **88**, 4286 (1966).
[30] L.G. Kuzmina, Y.S. Varshavskii, N.G. Bokii, Y.T. Struchkov, T.G. Cherkasova. *J. Struct. Chem. (Eng. Transl.)*, **12**, 593 (1971).
[31] E. Gutierrez-Puebla, J.V. Heras, A. Monge, E. Pinilla, A. Rodrigues-Roldan, J.M. Salvador. *Eur. Cryst. Meeting*, **9**, 178 (1985).
[32] F. Basolo, R.G. Pearson. *Prog. Inorg. Chem.*, **4**, 381 (1962).
[33] G.J.S. Venter. A crystallographic, computational and mechanistic study of rhodium enaminoketonato complexes. Unpublished Doctoral Dissertation, University of the Free State, Bloemfontein (2012).
[34] F. Shaheen, L. Marchio, A. Badshaha, M.K. Khosac. *Acta Crystallogr.*, **E62**, o873 (2006).
[35] Oxford Diffraction. *Crysalis CCD*, Oxfordshire Diffraction Ltd., Abingdon, Oxfordshire, UK (2005).
[36] Oxford Diffraction. *Crysalis RED*, Oxford Diffraction Ltd., Abingdon, Oxfordshire, UK (2005).
[37] Bruker. *SAINT-PLUS (including XPREP), (Version 7.12)*, Bruker AXS Inc., Madison, WI (2004).
[38] Bruker. *SADABS, (Version 2004/1)*, Bruker AXS Inc., Madison, WI (1998).
[39] G.M. Sheldrick. *Acta Crystallogr.*, **A64**, 112 (2008).
[40] L.J. Farrugia. *J. Appl. Cryst.*, **32**, 837 (1999).
[41] K. Brandenburg, H. Putz. *DIAMOND*. Release 3.0e. Crystal Impact GbR, Postfach 1251, D-53002, Bonn, Germany (2004).
[42] M.J. Frisch, G.W. Trucks, H.B. Schlegel, G.E. Scuseria, M.A. Robb, J.R. Cheeseman, J.A. Montgomery Jr., T. Vreven, K.N. Kudin, J.C. Burant, J.M. Millam, S.S. Iyengar, J. Tomasi, V. Barone, B. Mennucci, M. Cossi, G. Scalmani, N. Rega, G.A. Petersson, H. Nakatsuji, M. Hada, M. Ehara, K. Toyota, R. Fukuda, J. Hasegawa, M. Ishida, T. Nakajima, Y. Honda, O. Kitao, H. Nakai, M. Klene, X. Li, J.E. Knox, H.P. Hratchian, J.B. Cross, V. Bakken, C. Adamo, J. Jaramillo, R. Gomperts, R.E. Stratmann, O. Yazyev, A.J. Austin, R. Cammi, C. Pomelli, J.W. Ochterski, P.Y. Ayala, K. Morokuma, G.A. Voth, P. Salvador, J.J. Dannenberg, V.G. Zakrzewski, S. Dapprich, A.D. Daniels, M.C. Strain, O. Farkas, D.K. Malick, A.D. Rabuck, K. Raghavachari, J.B. Foresman, J.V. Ortiz, Q. Cui, A.G. Baboul, S. Clifford, J. Cioslowski, B.B. Stefanov, G. Liu, A. Liashenko, P. Piskorz, I. Komaromi, R.L.Martin, D.J. Fox, T. Keith, M.A. Al-Laham, C.Y. Peng, A. Nanayakkara, M. Challacombe, P.M.W. Gill, B. Johnson, W. Chen, M.W. Wong, C. Gonzalez, J.A. Pople, *GAUSSIAN-03*, Revision C.01, Gaussian, Inc., Wallingford, CT (2004).
[43] A.D. Becke. *J. Chem. Phys.*, **98**, 5648 (1993).

[44] P.C. Hariharan, J.A. Pople. *Theoret. Chim. Acta*, **28**, 213 (1973).
[45] M.M. Francl, W.J. Petro, W.J. Hehre, J.S. Binkley, M.S. Gordon, D.J. DeFree, J.A. Pople. *J. Chem. Phys.*, **77**, 3654 (1982).
[46] P.J. Hay, W.R. Wadt. *J. Chem. Phys.*, **82**, 299 (1985).
[47] V. Schurig, W. Pille, K. Peters, H.G. Von Schnering. *Mol. Cryst. Liq. Cryst.*, **120**, 385 (1985).
[48] T. Mochida, R. Torigoe, T. Koinuma, C. Asano, T. Satou, K. Koike, T. Nikaido. *Eur. J. Inorg. Chem.*, **2006,** 558 (2006).
[49] J.G. Leipoldt, L.D.C. Bok, S.S. Basson, J.S. Van Vollenhoven, T.I.A. Gerber. *Inorg. Chim. Acta*, **25**, L63 (1977).
[50] Y.S. Varshavsky, M.R. Galding, T.G. Cherkasova, I.S. Podkorytov, A.B. Nikol'skii, A.M. Trzeciak, Z. Olejnik, T. Lis, J.J. Ziolkowski. *J. Organomet. Chem.*, **628**, 195 (2001).
[51] J. Conradie, T.S. Cameron, M.A.S. Aquino, G.J. Lamprecht, J.C. Swarts. *Inorg. Chim. Acta*, **358**, 2530 (2005).
[52] V. Schurig, H. Gaus, P. Scheer, L. Walz, H.G. Von Schnering. *Angew. Chem., Int. Ed.*, **28**, 1019 (1989).
[53] F. Huq, A.C. Skapski. *J. Cryst. Mol. Struct.*, **4**, 411 (1974).
[54] V. Schurig, W. Pille, W. Winter. *Angew. Chem., Int. Ed.*, **22**, 327 (1983).
[55] A. Brink, H.G. Visser, A. Roodt, G. Steyl. *Dalton Trans.*, 5572 (2010).
[56] J. Conradie, G.J. Lamprecht, A. Roodt, J.C. Swarts. *Polyhedron*, **23**, 5075 (2007).
[57] K.H. Hopmann, N.F. Stuurman, A. Muller, J. Conradie. *Organometallics*, **29**, 2446 (2010).
[58] G.J.J. Steyn, A. Roodt, J.G. Leipoldt. *Inorg. Chem.*, **31**, 3477 (1992).